

Article

Electrical, Thermal and Optical Parametric Study of Guided Ionization Waves Produced with a Compact μ s-Pulsed DBD-Based Reactor

Kristaq Gazeli ^{1,2,*} , Le Thanh Doanh ¹, Bernard Held ^{1,†} and Franck Clément ¹

¹ CNRS/Univ. Pau & Pays de L'Adour, Institut des Sciences Analytiques et de Physico-Chimie pour l'Environnement et les Matériaux–MIRA, UMR 5254, 64000 Pau, France; doanhlh@epu.edu.vn (L.T.D.); bernard.held24@orange.fr (B.H.); franck.clement@univ-pau.fr (F.C.)

² LPGP, CNRS, Univ. Paris-Sud, Université Paris-Saclay, 91405 Orsay, France

* Correspondence: kristaq.gazeli@u-psud.fr; Tel.: +33-0169-156-570

† This author is a retired professor from Univ. Pau & Pays de L'Adour.

Received: 22 November 2017; Accepted: 20 December 2017; Published: 25 December 2017



Abstract: Atmospheric pressure guided ionization waves (GIWs) that are driven by ns/ μ s-pulsed high voltages, are promising tools in the biomedical field allowing for the effective production of reactive species and metastables without thermal damages of the specimens that are exposed. In most cases, plasma is produced in noble gases using dielectric barrier discharge (DBD) devices of more-or-less sophisticated geometries. In this study, a compact low-cost DBD reactor of very simple geometry is presented. It is fed with pure helium and driven by positive μ s-pulsed high voltage (amplitude: 4.5–8 kV, pulse width: 1–10 μ s) of audio frequencies (5–20 kHz), while it operates consistently for long time periods in a wide range of conditions. The produced plasma exhibits propagation lengths up to 4 cm and rich chemical reactivity is established outside the reactor, depending on the device's experimental parameters. Besides, the dielectric tube's temperature during plasma operation is an important factor, which is linked to the plasma characteristics. This temperature and its variations are thoroughly investigated herein, along with GIWs electrical features versus the electrical parameters of the pulsed power supply. Accordingly, it is demonstrated that not all of the operational windows are adequate for thermal-free operation and suitable operating conditions of this system are proposed for diverse applications, such as biomedical (low gas temperature is a prerequisite) and surface treatments of solid materials (low temperatures are not required).

Keywords: atmospheric pressure plasma jet; guided ionization waves; guided streamers; biomedical applications; non-thermal plasma

1. Introduction

The interesting physicochemical properties of the so-called “Atmospheric Pressure Plasma Jets” (“APPJs”) have been widely studied by many groups and different reactor designs have been proposed over the last years for their production [1,2]. The latter setups are based on the DBD (Dielectric Barrier Discharge) principle referring mainly to linear-field, coaxial, and single electrode geometries. The use of dielectric layers and alternative high voltages (ns– μ s range) defines the characteristics of the discharge. A build-up of charges on the dielectric surfaces induces an electrical field, which is opposite to the external one, limiting thus the discharge current and avoiding any transition to arc. Although “APPJs” appear as uniform luminous “plumes” by naked-eye observation, it has been demonstrated recently that they consist of ultrafast discrete “plasma bullets” or, more correctly in physical terms, guided streamer-like ionization waves [3–9], which are guided by the dielectric material (usually cylindrical) and the channel of a preselected noble gas (usually helium or argon).

Among other advantages of the Guided Ionization Waves—GIWs (selectivity, portability, repeatability, low relative production cost, etc.)—the operation at atmospheric pressure is particularly interesting, since it has opened new horizons for their implementation in biomedicine [10,11]. Due to plasma propagation in the atmospheric air, highly reactive species are formed in GIWs such as O, OH, H₂O₂, O₃, NO, etc. [12]. Another stimulating feature is that plasma chemistry is driven by electrons, while the heavy particles remain at low energies and the global gas temperature is kept near to the room one [6,13–19]. For biomedical applications, this is an important factor and it must be kept less than 40 °C [10], otherwise it can cause irreversible damages to the organisms that are subjected to treatment. In most of the cases, a stable “plasma plume” of variable length up to few cm is obtained, while there are options of generating GIWs within microtubes [20] and transferring it at distances of up to few meters by adapting appropriate dielectric tubes at the exit of the reactor [21,22]. These possibilities allow direct/indirect application on living cells and/or tissues, which can be found at different positions downstream of the reactor. For accurate results, special attention should be paid for the investigation of possible modifications of GIWs features due to the presence of different samples (conductive/insulating grounded or at floating potential).

Different groups have been focused to the characterization of GIWs devices by studying the impact of various parameters on the plasma properties in the free-GIW case (i.e., the plasma is not in contact with a target). A short review of these works is given right below.

Jarrige et al. [16] studied experimentally the dynamic behavior of “plasma bullets” that are produced in helium with a DBD reactor (dielectric: quartz), driven by microsecond pulsed high voltage (μ PHV). Even if two discharges were formed in the inter-electrode section per pulse, only one “bullet” was detected. Its velocity and diameter increased with the HV amplitude, also enhancing significantly the electron energy and active species generation. The discharge current depended strongly on the HV amplitude, while the gas temperature was rather low and independent on the voltage amplitude, making this device suitable for biomedical applications.

Zhu et al. [17] investigated experimentally the propagation dynamics of guided ionization waves generated in helium with a coplanar DBD reactor (dielectric: quartz) driven by sinusoidal HV. The streamer-like behavior was confirmed and the influence of external fields (electric/magnetic) on the propagation of the GIWs was revealed. Moreover, a floating metal ring did not affect the GIWs length, which did not happen when the ring was powered with a DC potential (positive voltages improved the length, while the negatives ones prevented its propagation).

A DBD reactor (dielectric: pyrex) driven by μ PHV was employed by Karakas et al. [23] to study the dynamics of a helium “plasma jet” and its corresponding current, also revealing a streamer-like behavior. In their case, the formation of a secondary discharge inhibited the “bullet’s” propagation. Besides, the “plasma jet’s” maximum current decreased linearly with the distance, reaching minimum values of about 4 mA at a distance of 30 mm downstream of the reactor.

In another work, Nastuta et al. [18] used a DBD reactor operating with helium (dielectric: quartz, voltage waveform: μ PHV) to produce and characterize electrically/optically a room-temperature “plasma jet” as potential source for biomedical applications. The “plasma bullet” formation and the rich chemical reactivity were confirmed. Additionally, the development of a localized plasma structure on a human finger (replica of a tissue) was revealed, which was sustained by a current that was flowing through it. The amplitudes of these currents depended on the finger’s distance from the reactor, while they were in the range of values that were adopted in well-known medical procedures (e.g., electrotherapy). In contrast with the free-GIW, the wavelength-integrated light signals resulting from the interface GIW-finger were widened and followed relatively well the dynamics of the current flowing through the finger. Additionally, enhanced production of the NO_γ emission (220–280 nm) was measured only when the GIWs were in contact with the fingertip. The same reactor was studied recently by the latter group [24]. The HV parameters (amplitude, frequency, pulse duration, and polarity) were tuned and the electrical parameters of the “plasma jet” and its geometric characteristics (i.e., current, length, diameter, total volume) were controlled in terms of biomedical applications.

The effect of the voltage waveform (i.e., ns-pulse, μ s-pulse and rectangular form) on the features of a helium “plasma jet”, was considered by Uchida et al. [25] using a similar reactor with the previous ones (quartz dielectric). The “plasma jet’s” length was increased more-or-less sharply with the voltage amplitude (4–10 kV), depending on the voltage waveform. For μ s-pulse and rectangular signals, a visible “jet” was obtained at 4.5 and 5.5 kV respectively, while for ns-pulse, it was visible only after 7 kV. The power consumption and the production of reactive species depended also on the voltage type/amplitude.

Finally, Yonemori et al. [26] studied the effect of the voltage’s polarity on the propagation and reactive species production efficiency of a helium “plasma jet” generated with a linear-field reactor (dielectric: quartz) driven with μ PHV. It was observed that the voltage’s polarity affected, not only the plasma propagation, but the density of the reactive species produced as well.

The above interesting works refer to DBD reactors with two-electrodes of variable width, forming the so-called linear-field arrangement. Other studies, referring to similar designs do exist as well [27–31]. Although, the electrodes that are used therein are in the form of very thin rings, which are entirely enclosed in the dielectric material, thus avoiding any contact with the atmospheric air for better insulation. Besides, setups using one single electrode have been also proposed [19,32–36], which in some cases, are directly compared with linear-field configurations in the same study [28]. In most of these setups, quartz is used as dielectric material and helium as the process gas, which are quite reliable.

Concerning the GIWs-target system, extensive works referring in helium and argon GIWs have been reported recently. For instance, Darny et al. [37] studied a μ s-pulsed helium “plasma gun” impinging on a conductive target. The presence of the target lead to a glow discharge regime, which did not occur for the free-GIW. In contrast with the free-GIW case, helium metastables density was enhanced inside the plasma plume and the capillary tube. Besides, drastic enhancement of reactive species (NO, OH, O, ...) production was detected for the GIWs-target system. Yamada et al. [38] studied both helium and argon GIWs in contact with a copper plate and a mouse. A noticeable increase of reactive species emission was observed near the conductive target, which was enhanced significantly with the decreasing distance between the nozzle and the target. On the other hand, the temperature of the mouse surface during the treatment, never exceeded 40 °C for both types of GIWs. Es-Sebbar et al. [39] investigated an ns-pulsed argon GIW in contact with a floating-potential glass surface. It was found that the argon metastables density, measured at a distance of 3.65 mm from the dielectric tube orifice, was doubled in respect to the free-GIW case. In another work of the latter group [40], the temperature of the glass surface (measured with an infrared camera) and the gas temperature (estimated via OES) were found to be below 40 °C when the glass was maintained at floating potential. But, it was increased up to 2-fold when the plate was connected to the ground.

For the GIWs-based applications, the processes happening during sample treatment are determined by the system’s internal variables, i.e., the densities of electrons, radicals/ions and the temperatures of neutral/ionized species (rotational, vibrational, electron) that were produced in the gaseous phase and at the plasma/target interface. For each GIW, there is a strong connection between the internal variables and the external ones (voltage waveform and amplitude, gas type and flow rate, frequency, etc.), which has been well-demonstrated by different groups (see references listed in the previous paragraphs). Understanding the connection between the internal and the external variables appears to be crucial for the development of adequate microplasma devices designed for biomedical applications and surface treatments of inert materials. The problem in this case is twofold. Firstly, the internal parameters of GIWs must be correctly evaluated and controlled for the free-GIW case. This way, adequate operational windows may be defined, assuring the production of sufficiently high reactive species densities at low gas temperatures. The latter is crucial for the treatment of heat-sensitive biological tissues. Secondly, under the above operational windows, the GIWs-target system should be considered and studied as a whole. In this case, the discharge dynamics and gas temperature could be drastically modified due to the presence of a sample/tissue (each sample exhibits

different properties such as conductivity, humidity, porosity, etc.). Besides, in the case of exposed living samples or dynamic systems, their responses will induce modifications on the plasma features during treatment, which need to be considered for the optimization of the processes.

Following the above principles/studies, this work consists a systematic experimental investigation (electrical, thermal, and optical/spectroscopic) of helium GIWs (target-free) and their optimization for biomedical and surface treatment applications. In numerous publications, GIWs are considered as a-priori cold and there is lack of systematic thermal studies performed on this kind of plasmas. The notion of temperature is crucial for biomedically-oriented GIWs since, for values higher than 40 °C, the organic tissues can be irreversibly damaged. Furthermore, the temporal modification of the dielectric tube temperature during plasma operation is an important factor, which to our knowledge has been poorly investigated. It must be always known for better understanding/controlling the thermal processes that are involved in the reactor, which can highly modify its reliable operation, and thus the characteristics of GIWs, especially at elevated temperatures.

This topic highly motivates the present work, which is proposed as an extension of the already published ones in the literature concerning target-free GIWs. Its main goal is to contribute further to the optimization and the control of GIWs features (especially the thermal ones) before their implementation on various applications in order to investigate subsequently the dynamics of GIW-target systems. A compact low-cost DBD reactor of very simple geometry is used for the production of GIWs. It uses alumina as a dielectric, it is designed to operate both with μ s-pulsed (demonstrated herein) and sinusoidal HV [32], and it can be employed both for fundamental studies (experimental/numerical, see [32] for instance) and microplasma-based applications. The temporal variation of the dielectric tube temperature is thoroughly investigated versus the electrical parameters of a positive μ s-pulsed power supply. Besides, other plasma features are extensively studied to support the thermal studies, such as its propagation length, electrical characteristics (current/charge), and reactive species production. The possibility of the system's optimization in terms of current, reactive species production, and (especially) temperature, is demonstrated and suitable operational windows are proposed for applications in biology and medicine and, in analyzes of inert materials. Accordingly, it is demonstrated that not all of the operational windows are adequate for thermal-free operation. These results contribute further to the better understanding and control of the complex operation of GIWs and to the design of microplasma devices of specific characteristics (i.e., short/long plasmas of enhanced/moderate chemical reactivity at low/high temperatures) for targeted plasma-based applications.

2. Materials and Methods

The conceptual view of the reactor employed for the production of GIWs in this work is illustrated in Figure 1. The main body of the device consists of a cylindrical capillary ceramic tube (Al_2O_3 , $\epsilon_r = 9.75$ mm in length, 1.14 and 2.5 mm inner and outer diameter, respectively). Helium of high purity (N50) is chosen as the process gas, and it is injected in the ceramic via a polymeric tube that is tightly connected at the inlet of the dielectric with a metallic hollow adaptor (see Figure 1). The internal wall-surface of the adaptor was filled by a hollow polymeric tube, into which the polymeric-and-dielectric tubes were tightly adjusted. This way, the metallic connector was not in direct contact with the other tubes and the gas inside them. The connector was maintained always at floating potential, and it did not alter the discharge ignition under the operating conditions that were considered in this work. However, an upstream propagation was observed under most of the conditions and the contribution of the metallic connector on this phenomenon cannot be excluded. The gas flow rate (Q) is controlled with a volume gas flow meter (ANALYT-MTC, Messtechnik GmbH, Colmar, France), and it is maintained constant at 3 slm (standard liters per minute) during all of the experiments. Two aluminum foil electrodes were glued on the external surface of the dielectric tube at a fixed distance between them of 15 mm. The first one (10 mm long, placed 10 mm away from the dielectric nozzle) is connected to the circuit ground and the second one (10 mm long, placed 35 mm away from the nozzle) to the output of a (pulsed positive) high voltage power supply. To avoid any discharge formation

between the two electrodes outside the dielectric tube, the space between them is filled with a thick layer of a standard insulating electric tape (see Figure 1). The HV pulses are variable in amplitude ($V_p = 4.5\text{--}8\text{ kV}$, rising slope: 150 V/ns), duty cycle ($d = 1\text{--}10\%$, i.e., the ratio of the pulse width to the voltage period: t_{ON}/T in Figure 1), and frequency ($f = 5\text{--}20\text{ kHz}$). The applied voltage and the DBD total current were measured using a high voltage divider (Tektronix P6015A, 75 MHz, Tektronix, Paris, France) and a wideband current probe (Tektronix CT2, 1.2 kHz to 200 MHz, 500 ps rising time, 1 V/A into 50 Ohms), respectively. The total current consists of the discharge's current (conduction) superimposed to the displacement one (capacitive coupled electrical circuit) and it was measured at the grounded electrode (see Figure 1). The voltage and current waveforms were monitored simultaneously in a wideband digital oscilloscope (Tektronix TDS3054B, 5 Gs/s, 500 MHz).

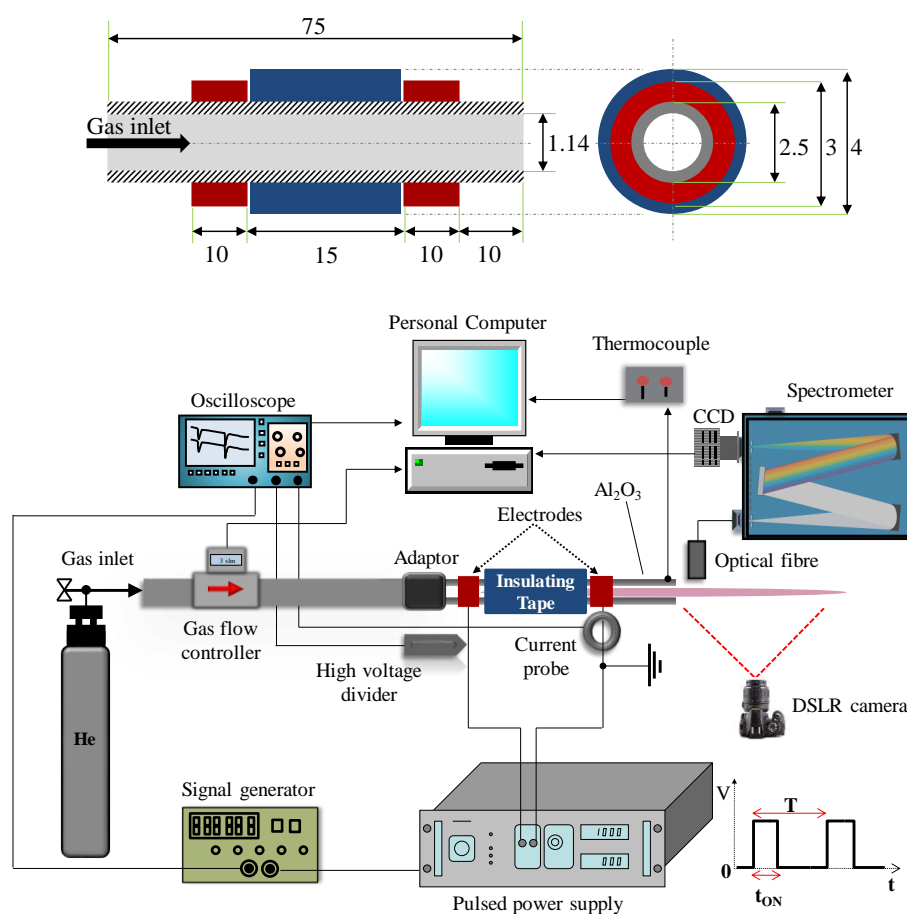


Figure 1. Upper figure: side section (left) and front view (right) of the dielectric barrier discharge (DBD)-based linear-field reactor employed along with the detailed dimensions (not in scale) of its components. Lower figure: configuration of the reactor (shown in the center of the image) and experimental arrangement of the peripheral devices used for the analysis (electrical/thermal/optical) of the produced guided ionization waves (GIWs) (pink/violet “plume” in the figure).

For the measurement of the dielectric tube temperature, a thermocouple (National Instruments 9211, Nanterre, France) is mounted near to its orifice (see Figure 1), allowing for real time monitoring in a personal computer. Special attention is paid to avoid possible perturbations on the GIWs electrical characteristics, by placing it as it is shown in the lower frame of Figure 2. This method is the same with the one used in [41] and it allows reliable control of the thermal processes evolved during the reactor operation. The overall error on the measured temperature (i.e., error of the device and the statistical error is estimated to be $\pm 5\text{ }^\circ\text{C}$). Representative temporal profiles of the tube temperature

within the first three minutes (t_s , i.e., the time required for the reactor to reach in a steady-state regime) after the plasma ignition and for different HV amplitudes are illustrated in the upper frame of Figure 2. Initially, the temperature is the same with the room one (20 °C). After the plasma ignition, it increases exponentially due to the increase of the current carriers in the tube reaching eventually a saturation value (T_{sat}) at the end of the period t_s . The ceramic tube is then heated continuously at T_{sat} , and a constant regime is obtained for the reactor mechanical parts. T_{sat} is measured herein under all of the experimental conditions, and it is plotted versus the system operating parameters (see results section).

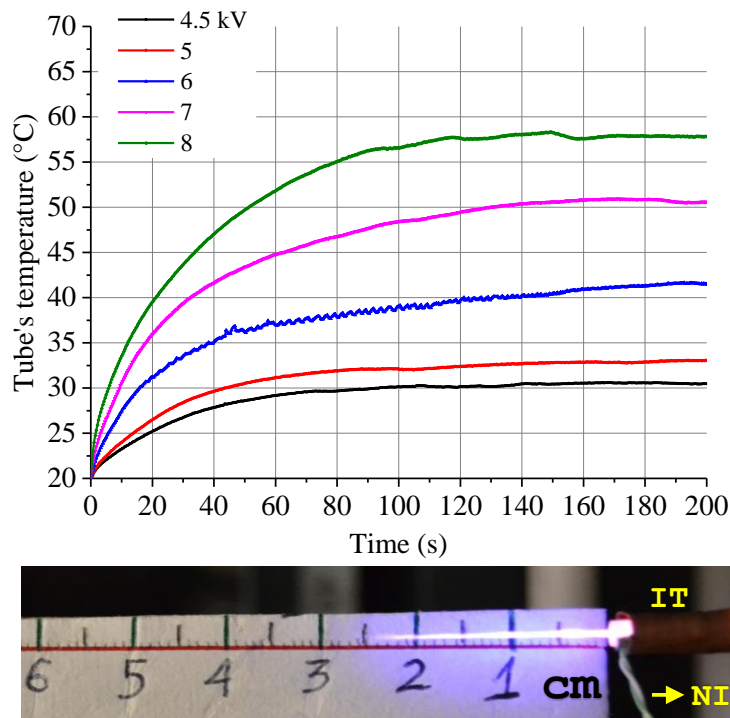


Figure 2. Upper frame: Temporal evolution of the tube temperature measured with a thermocouple (see NI in the lower frame) within the first three minutes after the discharge ignition. **Lower frame:** measurement method of the GIWs length using a DSLR camera (exposure time: 5 ms) and a calibrated paper ruler. NI denotes the thermocouple cable and IT signifies the insulating tape, which is used to maintain the NI cable in contact with the tube and to avoid perturbations to the plasma. Operating conditions: $Q = 3$ slm, $V_p = 8$ kV, $d = 2\%$, $f = 10$ kHz.

Besides, the length of the GIWs was measured similarly with [42] by using a high-definition DSLR camera (Nikon® D3100, Nikon, Paris, France) and a calibrated paper ruler (use of metallic ruler was avoided to avoid possible perturbations on the dynamics of GIWs), which are placed perpendicularly (~ 100 cm away) and parallelly (20 cm away) to the plasma axis, respectively (see indicative snapshot in the lower frame of Figure 2). The emission intensities of various reactive species that were formed outside the reactor were identified/studied in a wide wavelength range (300–800 nm) via a high-resolution spectrometer (JOBIN YVON 1000 M, 1200 grooves/mm grating blazed at 500 nm, Horiba Scientific, Longjumeau, France), equipped with a CCD camera. The emitted light was collected via a wideband optical fiber, which was placed perpendicular to the dielectric tube axis (8 mm away from its nozzle). Light measurements were integrated spatially (see results section for details) and temporally (within 1500 voltage pulses). OES was applied herein only for qualitative analysis, since the spectral efficiency of the system at different wavelengths was ignored.

Figure 3a illustrates representative electrical waveforms (voltage/current) recorded within a voltage pulse (plasma on). The DBD total current (conduction and capacitive) oscillates during the voltage rise/fall times due to the electrical circuit parasitic components (R-L-C circuit). Except for

these oscillations, the formation of two distinct current impulses is clearly observed, i.e., a positive and a negative one corresponding to the rising and the falling voltage slope, respectively (see Figure 3a). These are indirectly associated with the plasma current in the inter-electrode region. The positive impulse refers to a primary discharge that is formed in the reactor, with characteristics depending strongly on the system operating parameters [16,25,43,44]. It is now well known that this primary discharge is due to the development of a guided ionization wave or guided streamer [3,4]; it is formed in the DBD region once the space charge electric field becomes comparable to the external one, and it propagates fast (velocities up to some 100 s km/s) outside the reactor, being confined in the noble gas channel. The negative impulse refers to a secondary discharge, which in the case of linear-field GIWs, is attributed to the release of charges accumulated in the dielectric tube during the rising slope of the voltage [16,23]. A time lag (Δt_{GIWs}) is established between the zero-crossing point of the positive current impulse and the rising voltage edge. The corresponding Δt_{GIWs} in the case of negative impulse is negligible under our experimental conditions, which is in agreement with other published works [16,23,42]. Hereafter, the results section will refer to the peak value (I_{Peak}) of the positive current impulse, its corresponding accumulated charge (Q_{main} , obtained through integration of the current impulse over time), and the time lag Δt_{GIWs} (see Figure 3b for definition). These are characteristic of the influence of the system electrical parameters on the electrical properties of GIWs.

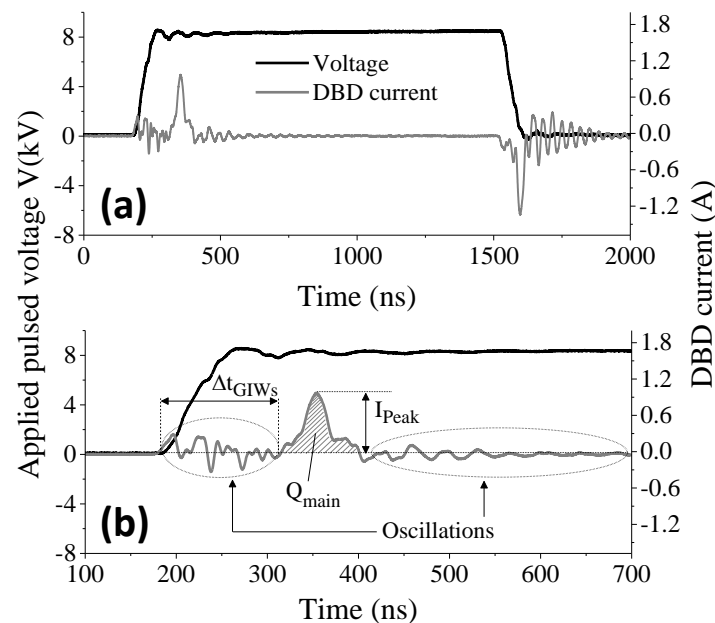


Figure 3. Typical waveforms of the applied voltage (black) and the corresponding DBD total current (grey) (a) within a voltage pulse and (b) during the voltage rising time. The effect of the system electrical parameters on the positive current impulse is studied by considering three quantities: its peak value (I_{Peak}), the total amount of accumulated charge (Q_{main} , shaded area below the impulse) and the time delay in respect with the onset of the voltage pulse (Δt_{GIWs}). Operating conditions: $Q = 3$ slm, $V_p = 8$ kV, $d = 2\%$ and $f = 15$ kHz.

3. Results and Discussion

In this section, the effect of the electrical parameters (i.e., V_p , d and f) on the quantities I_{Peak} , Q_{main} and Δt_{GIWs} of the positive current impulse (see Figure 3b), on the length of GIWs (L_{GIWs}) and on T_{sat} is thoroughly investigated. Firstly, the impact of the voltage amplitude and the duty cycle are discussed in the Section 3.1, followed by the effect of the frequency (Section 3.2). Finally, in Section 3.3, the optical emission characteristics of the GIWs are analyzed and the effect of V_p on the intensities of principal (re)active species is studied.

3.1. Effect of the Voltage Amplitude (V_p) and Duty Cycle (d) on I_{Peak} , Q_{main} , Δt_{GIWs} , L_{GIWs} and T_{sat}

Figure 4 shows representative waveforms of the total DBD current during the rising (left) and the falling (right) slope of the pulsed voltage for different voltage amplitudes. As it was previously mentioned, the tuning of V_p does not affect the Δt_{GIWs} of the negative impulse, which is clearly demonstrated in the right frame of Figure 4. Identical behaviors were remarked in other studies, as well concerning linear-field [16] and single-electrode [42] setups. Jarrige et al. [16] observed via ICCD measurements that the secondary discharge appeared in the DBD at the end of the voltage pulse, without any evident formation of a second plasma “bullet”. Besides, I_{Peak} and Q_{main} related with this impulse, change clearly with V_p (see right frame of Figure 4). Although, the study of the system parameters influence cannot be realized systematically, the present work will focus only on the positive current impulse (left frame of Figure 4). Its variations are related with the ones of excited species formed in the GIWs, such as the helium at 706.5 nm (i.e., 3^3S-2^3P transition), which was demonstrated by different groups [16,25]. Since these species are formed via electron impact excitation, they are indicative of the modifications of the electron properties in the plasma, and thus, the ones of the discharge and the DBD total current. I_{Peak} , Q_{main} and Δt_{GIWs} of this impulse depend clearly on the voltage amplitude in our case. The signal oscillations that were recorded between 200 and 350 ns are almost the same at different V_p values and they are ignored. With increasing V_p from 4.5 to 8 kV, Δt_{GIWs} shrinks considerably and I_{Peak} becomes noticeably higher (about 9-fold increase is observed). At elevated voltage amplitudes, the externally-applied electric field is strengthened and the reduced electric field in the DBD is also increased. Thus, a higher amount of electrical energy is delivered in the reactor. The electrons gain more kinetic energy as compared with the one at lower voltage amplitudes, which leads eventually to faster excitations/ionizations both in the inter-electrode section and in the gaseous channel. As such, the current impulse arrives faster in time with an increasing V_p and “guided streamers” accelerate at higher V_p values [16], which was observed as well in a different electrode configuration [42] than the present one.

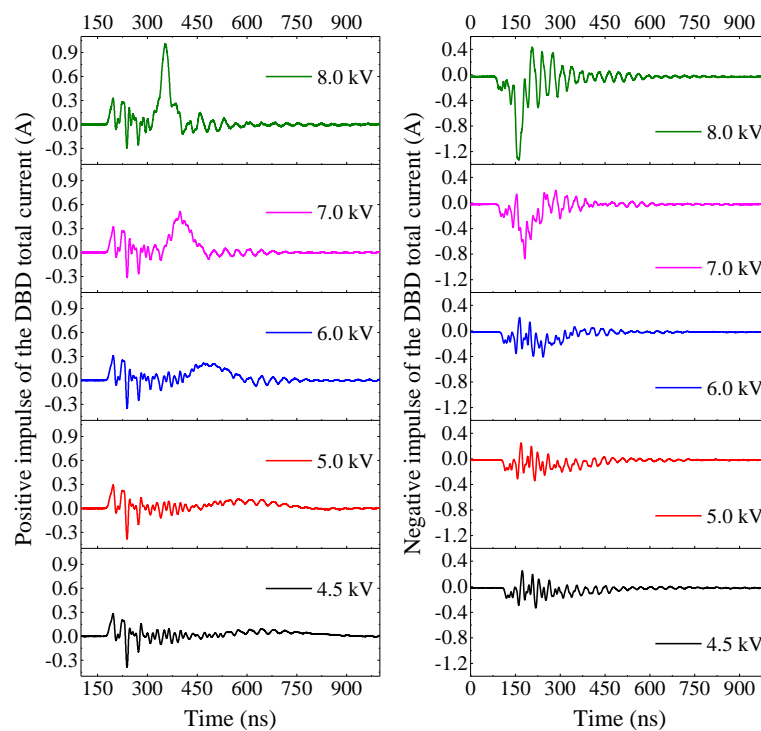


Figure 4. Total current of the DBD during the rising (left images) and the falling (right images) slope of the voltage versus the voltage amplitude. Operating conditions: $Q = 3$ slm, $d = 2\%$ and $f = 15$ kHz.

The variations recorded in the total current of Figure 4 are representative of the conduction current (i.e., plasma current) due to an amplification of the charge carriers (see below) under the action of the elevated reduced electric field. Hereafter, the influence of V_p on the values of I_{Peak} , Q_{main} , and Δt_{GIWs} will be studied systematically, along with the variations of L_{GIWs} and T_{sat} . The corresponding variations of I_{Peak} , Q_{main} , and Δt_{GIWs} will be shown only for $V_p \geq 6$ kV, since at lower amplitudes, the signals are comparable with the circuit oscillations, which could induce significant errors on the accurate determination of the above quantities.

Figure 5 shows the variations of I_{Peak} , Q_{main} and Δt_{GIWs} versus V_p for different duty cycles at $f = 15$ kHz. I_{Peak} (Figure 5a) is independent on the duty cycle within the range of values examined herein. On the other hand, the increment of the applied voltage from 6 to 8 kV induces an almost linear increase of the total current from ~ 0.2 to ~ 1 A, respectively (for $V_p \leq 5$ kV, I_{Peak} is lower than 0.15 A, see Figure 4), similar comportment with other published works [16,42]. This fact may be attributed to an amplification of the electron avalanches in the gaseous channel due to higher electron energy [25] at higher voltage amplitudes. As suggested by Nastuta et al. [24], the variations of the maximum current could be associated to the ones of excited species (N_2^+ , O, OH, ...), the production of which is closely related with the electronic properties (density, temperature) and the composition of the gaseous medium. In the present study, the total current is measured in the DBD discharge. It is thus expected that it is larger than the actual plasma (conduction) current in the DBD [16,27] and the current of GIWs (I_{GIWs}) [23]. Indeed, I_{GIWs} is very low under our experimental conditions, especially at higher distances downstream of the reactor, which was verified by touching the plasma by the finger without any electrical shock. Regarding Q_{main} (i.e., time-integrated DBD current, see Figure 5b), it is independent on the duty cycle and it increases linearly with V_p , i.e., identical comportment with the total current. This behavior of I_{Peak} and Q_{main} for $d = 1\text{--}10\%$ was also observed by another group [42], although for a single-electrode configuration operating at 4 kHz and a much lower helium flow rate (0.5 slm). Between 6 and 8 kV, it varies from 23 to 35 nC, indicating significant magnification of the excitation/ionization processes in the gaseous channel. According to Nastuta et al. [24], this maximum value is obtained only after five minutes of plasma operation for a linear-field DBD reactor (quartz dielectric). In our case, Q_{main} obtained at 8 kV, is about twice higher than the one measured in [24]. This difference is attributed to the different geometric dimensions of the two reactors and the use of alumina as dielectric in our case, which results in higher currents as compared to the quartz. In contrast with the latter quantities, Δt_{GIWs} is clearly reduced with the increment of V_p . This is representative of a faster establishment of the discharge in the DBD due to more efficient excitation/ionization of the gas [16,25]. It means that the propagation velocity of the guided streamers is also amplified, which was confirmed in [16,29,30,44]. Depending on the duty cycle value, Δt_{GIWs} decreases from ~ 250 ns at $V_p = 6$ kV to ~ 100 ns at $V_p = 8$ kV, values that are in the range of the ones published in the bibliography [16,25]. These results demonstrate also clearly that low duty cycle values highly favorize the fast development of the discharge, which correlates with [43,45] even if they refer to different electrode setup and operating gas.

Figure 6 illustrates the effect of V_p on L_{GIWs} for different duty cycles at $f = 15$ kHz. As it can be seen, even a low voltage amplitude of 4.5 kV is high enough to generate GIWs with a length of 0.25, 0.5, 1, and 2 cm, corresponding to $d = 1.5\%$, 2%, 5%, and 10%, respectively. Instead, at $d = 1\%$ no visible "plasma jet" is detected outside the tube for $V_p \leq 5$ kV. L_{GIWs} increases almost linearly with V_p , obtaining its maximum value of ~ 4 cm at $V_p = 8$ kV, and $d = 1\text{--}2\%$ (a saturation value seems to be established between 7 and 8 kV for $d = 1.5\text{--}2\%$). Analogous behavior has been observed by other groups in similar [24,25,31] and different [42] μs -pulsed driven GIWs; it could be related with the increase of the energy transferred in the gaseous channel, leading to longer GIWs for a smaller helium mole fraction [31]. Besides, two bends are distinguished among the low and the high d values identically with [42], where a single electrode APPJ device was reported. For $d = 1\text{--}2\%$, L_{GIWs} increases sharply with V_p , while for $d = 5\text{--}10\%$, the corresponding slopes are clearly slower, resulting in shorter lengths for $V_p \geq 7$ kV. Further, L_{GIWs} depends slightly on the duty cycle for $d = 5\text{--}10\%$, which is not

the case for $d \leq 2\%$. Indeed, L_{GIWs} grows progressively with an increasing d between 1% and 2%. Another interesting result is that, for $V_p = 4.5$ and 5 kV, L_{GIWs} is higher at $d = 5\text{--}10\%$ as compared with the lower d values, while the situation inverses for $V_p > 6$ kV. These results suggest that under our experimental conditions, the GIWs length is highly affected by the duty cycle (especially at low values) and the voltage, while the optimum d and V_p values in terms of long plasma propagation are 2% and 7–8 kV, respectively. For plasma-based applications, it means that controllable production of GIWs can be achieved at different distances downstream of the reactor, i.e., probable positions of samples. It is underlined that the plasma properties (e.g., production of reactive species) may be strongly changed due to the characteristics of the sample that is exposed to the GIWs (conductivity, humidity, porosity, etc.), which has been shown in recent publications [37–40].

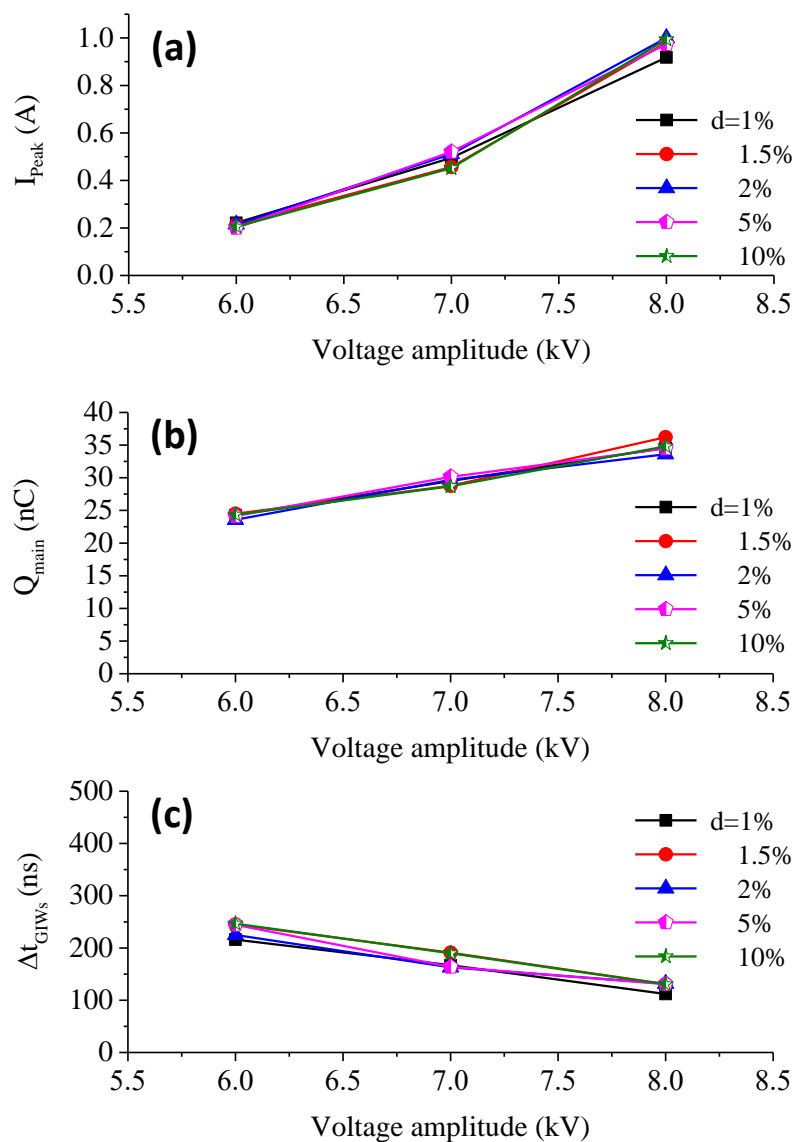


Figure 5. (a) Peak value of the positive current impulse (I_{Peak}); (b) total amount of charge (Q_{main}) of the positive current impulse during the rising slope of the voltage; and (c) time delay (Δt_{GIWs}) between the onset of the voltage pulse and the appearance of the positive current impulse, as functions of the voltage amplitude for different duty cycles ($Q = 3$ slm and $f = 15$ kHz).

Since many of the plasma-based DBD systems are meant to be used in biomedicine, the notion of temperature is very important. Different groups have proposed biocompatible reactors in terms of

gas temperature [14–16,24], for which the temperature modification of the reactor mechanical parts is not considered. The effect of V_p on the dielectric tube temperature (T_{sat} , see Figure 2) is thoroughly studied herein. T_{sat} is supposed to be important for two reasons: (i) it gives an indirect indication of the gas temperature variations inside the reactor and (ii) it allows for real-time monitoring of the thermal processes that are involved in the DBD and accurate definition of the reactor steady-state operational regimes (to avoid, e.g., possible malfunction of its mechanical parts, which can modify the GIWs features). Figure 7 shows the variation of T_{sat} as a function of the amplitude of the applied voltage for different duty cycles at $f = 15$ kHz. An increase of V_p induces an almost linear growth of T_{sat} for all of the duty cycles considered. Concerning the duty cycle effect, T_{sat} varies slightly between 1% and 2% for $V_p = 4.5$ –8 kV, while it increases for $d = 5$ –10% as compared with the lower d values, especially for $V_p > 6$ kV. It can reach up to a maximum value of 80 °C at $V_p = 8$ kV and $d = 10\%$, which is quite high for biocompatible systems, even for the reactor itself in terms of “harmless” operation. On the other hand, it can be lower than 40 °C for $V_p < 6$ kV, particularly at low d values. The latter increment of the temperature with V_p could be related with the increase of the electrical energy as it was stated above, leading to amplified current amplitudes (Figure 5a), which induce Ohmic effects (i.e., heating of the tube). Except the system optimization for biomedical purposes, these variations of T_{sat} offer valuable information for preventing the aging of the DBD reactor components, which could define the plasma features.

Based on the above results, it can be concluded that for a frequency of 15 kHz, the optimum operating conditions of the present GIWs system in terms of biomedical applications and reliable long-term operation, are the following: V_p from 4.5 to 6 kV and d between 1% and 10%. Within this operational window, T_{sat} remains lower than 40 °C, while the length of GIWs can be varied to reach specimens that are placed up to 3.5 cm downwards from the reactor. Appropriate operational windows can be obtained for all of the frequencies between 5 and 20 kHz, as it will be shown in the next subsection.

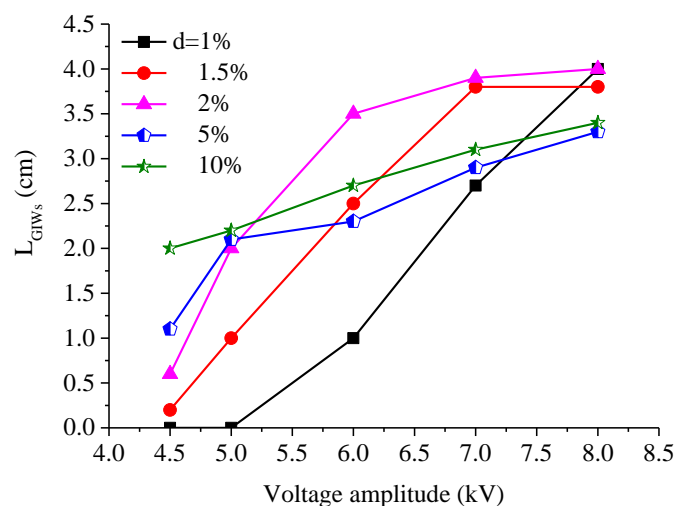


Figure 6. Length of the GIWs (L_{GIWs}) as a function of the voltage amplitude for different duty cycles. Operating conditions: $Q = 3$ slm and $f = 15$ kHz.

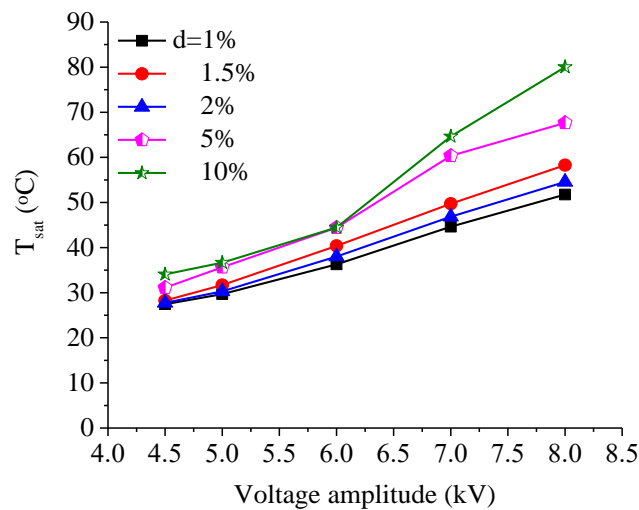


Figure 7. Maximum temperature (T_{sat} , see Figure 2 for definition) of the dielectric tube external surface as a function of the voltage amplitude for different duty cycles. Operating conditions: $Q = 3$ slm and $f = 15$ kHz.

3.2. Effect of the Pulse Frequency (f) on I_{Peak} , Q_{main} , Δt_{GIWs} , L_{GIWs} and T_{sat}

The effect of the pulse frequency on the I_{Peak} , Q_{main} , Δt_{GIWs} , L_{GIWs} , and T_{sat} , is herein studied for different V_p values at $d = 2\%$. This value is adopted hereafter, since it allows for the effective production of elongated GIWs at relatively low temperatures (see previous section). The pulse frequency is varied from 5 to 20 kHz and its influence on I_{Peak} , Q_{main} and Δt_{GIWs} , is illustrated in Figure 8a–c, respectively. An increase of the pulse frequency induces slight increase on the measured I_{Peak} (see Figure 8a) for $V_p = 8$ kV, which was also observed in [42] studying a single-electrode helium GIW. Besides, for all of the frequency values considered, I_{Peak} rises sharply with V_p (idem with the previous section). This is also the case for the total amount of charge Q_{main} , which rises from ~ 22 nC at 6 kV to ~ 35 nC at 8 kV, while it remains insensitive to the frequency increment (see Figure 8b). On the other hand, it is noteworthy that the positive current impulse (rising voltage slope) is obtained much faster at higher pulse frequencies (i.e., 50% decrease on Δt_{GIWs} from 5 to 20 kHz, see Figure 8c), indicating a noticeable acceleration of the guided streamers. Indeed, Walsh et al. [44] demonstrated that, with increasing frequency between 2.5 and 20 kHz, higher propagation velocities up to 2-fold can be achieved (2 cm outwards from the reactor) for the same GIWs. This behavior is also true for different reactor setups than the present one [42]. At higher frequencies, the time lag between successive guided streamers shortens and more seed electrons are available for upcoming avalanches [44]. The excitation of chemical species (metastables, radicals and ions, with lifetimes between 0.1 and 10 ms [42]) is enhanced as well, and their densities increase, thus contributing to the following discharge [4]. Consequently, excited/charged species are produced relatively faster and effectively between the electrodes and in the gaseous channel, which promotes an earlier discharge development (see Figure 8c).

The impact of the pulse frequency on the visible length of GIWs is depicted in Figure 9. For $V_p = 6$ –8 kV, L_{GIWs} follows a linear sharp increment in the range 5–15 kHz (from 1.5 to 3.5–4 cm, respectively). Then, a saturation seems to be established between 15 and 20 kHz for $V_p = 7$ –8 kV (maximum $L_{\text{GIWs}} = 4$ cm), while for $V_p = 6$ kV, a decrease is revealed at 20 kHz ($L_{\text{GIWs}} = 3.1$ cm). On the other hand, for $V_p = 5$ kV, L_{GIWs} grows slowly from 1.5 to 2 cm, corresponding to 5 and 15 kHz, respectively, while it falls down to 1 cm at 20 kHz. Finally, at $V_p = 4.5$ kV, L_{GIWs} is shrunk from 1 to 0.5 cm, corresponding to 5 and 15 kHz, respectively, while at 20 kHz, there is no visible “plasma plume” outside the reactor. The tendencies that are observed herein up to 8 kHz are in quite good agreement with the work of Nastuta et al. [24], where L_{GIWs} increased continuously with the pulse frequency in the range 0.5–8 kHz. From these results it is clear that there is a connection between the

GIWs length and the voltage pulse's frequency, while $f = 15$ kHz seems to be an optimal value for effective production of elongated GIWs within the range of voltage amplitudes considered herein. This is why this frequency value was chosen in the previous section to perform parametric studies versus the voltage amplitude and the duty cycle. Although, these results are not linked with the ones reported in [44], where L_{GIWs} appeared significantly longer at 20 kHz (~4.8 cm) in respect to 5 kHz (~3.5 cm), for $V_p = 4.6$ kV and a pulse width of 2 μ s. Besides, in the work of Xiong et al. [43], L_{GIWs} did not depend on frequency at all. The differences that were observed between these three DBD systems could be related to the dissimilar electrode configurations and dielectric materials used, while for a better understanding of these behaviors, more experimental/theoretical works are necessary.

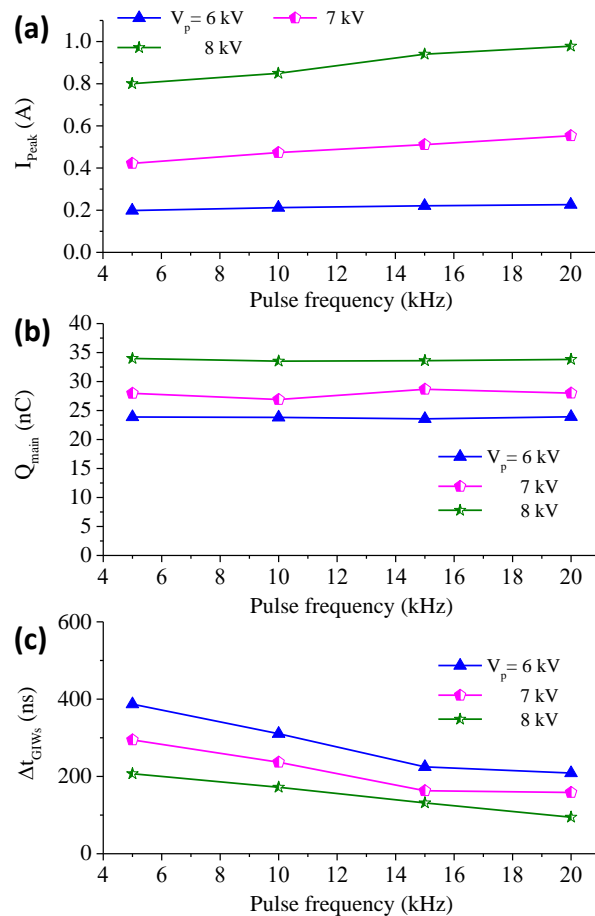


Figure 8. (a) Peak value of the positive current impulse (I_{Peak}); (b) total amount of charge (Q_{main}) of the positive current impulse during the rising slope of the voltage; and, (c) time delay (Δt_{GIWs}) between the onset of the voltage pulse and the appearance of the positive current impulse, as functions of the pulse frequency for different voltage amplitudes. Operating conditions: $Q = 3$ slm and $d = 2\%$.

Finally, the dependence of the dielectric tube temperature (T_{sat} , see Figure 2 for definition) on the pulse frequency is illustrated in Figure 10. The impact of the voltage amplitude on T_{sat} is clearly observed in good agreement with Figure 7, and a continuous increase is recorded from 25 up to 60 °C (corresponding to 4.5 and 8 kV, respectively). Concerning the frequency's effect on T_{sat} , the same tendency is recorded for all of the voltage amplitudes. From 5 to 10 kHz, T_{sat} increases from 25/40 ($f = 5$ kHz, $V_p = 4.5/8$ kV) to about 30/55 °C ($f = 10$ kHz, $V_p = 4.5/8$ kV). Then, it varies slightly between 10 and 15 kHz within a range of ± 3 °C. Finally, from 15 to 20 kHz, T_{sat} increases again from 26/55 ($f = 15$ kHz, $V_p = 4.5/8$ kV) to about 30/60 °C ($f = 20$ kHz, $V_p = 4.5/8$ kV). This increase may be related to a faster movement of electrical charges in the reactor at higher frequencies, which affects the

temperature of the GIWs [6], and, as a consequence, the T_{sat} . Furthermore, depending on the chosen value of V_p and the desired characteristics of GIWs for biomedical applications, it is possible to achieve T_{sat} values lower than 40 °C under all of the frequency values that are considered herein. On the other hand, it is shown that not all of the reactor functional windows are adequate for thermal-free operation. Except for the biomedicine, the present system could be adequate for other types of applications as well (e.g., processing of inert materials like dielectrics and polymers).

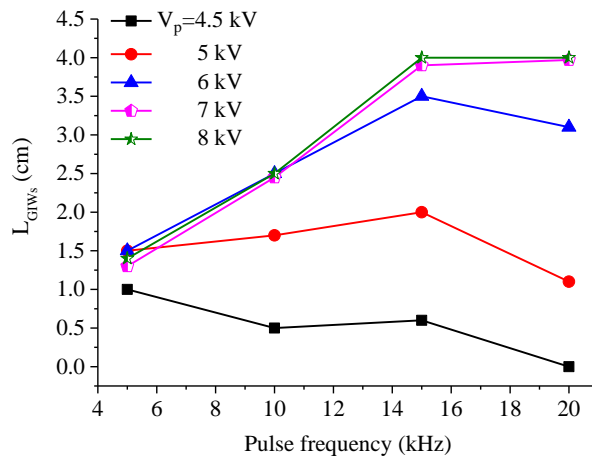


Figure 9. Length of GIWs (L_{GIWs}) as a function of the pulse frequency for different voltage amplitudes ($Q = 3$ slm and $d = 2\%$).

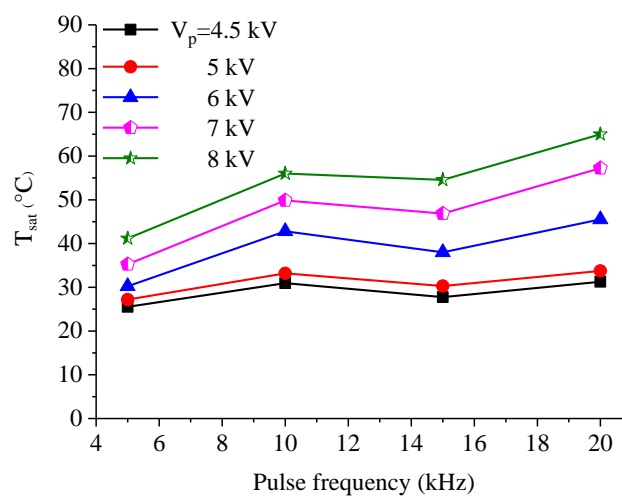


Figure 10. Maximum temperature (T_{sat} , see Figure 2 for definition) of the dielectric tube external surface as a function of the frequency for different voltage amplitudes ($Q = 3$ slm and $d = 2\%$).

3.3. Optical Emission Characteristics of GIWs

According to the previous sections, the GIWs electrical (I_{Peak} , Q_{main} , and Δt_{GIWs}) and thermal (T_{sat}) characteristics depend strongly on the parameters of the pulsed power supply (voltage amplitude, duty cycle, and frequency). Based on these results, appropriate operational windows can be defined to avoid reactor malfunctioning due to high operational temperatures and to produce on-demand GIWs for implementation in the biomedical and other research fields. As it is suggested by recently published references [37–40], the presence of a target (biological and/or inert material) may strongly modify the GIWs dynamics, temperature, and generated reactive species densities. Towards this direction, an effective control of the above parameters, and especially the temperature and the reactive species

formation in the free-GIW case, appears to be crucial for better understanding the GIWs performance on various specimens (mostly biomedical). As it was shown by different groups, the latter can be tuned (free-GIW case) by varying the system parameters [6,15,16,25,43]. In this section, effective production of emissive reactive species is achieved even at the lower voltage amplitude of 4.5 kV ($L_{GIWs} = 0.5$ cm), which is demonstrated below via optical emission spectroscopy measurements (see Figure 11).

Figure 11 depicts a typical wide emission spectrum of the GIWs recorded at $V_p = 4.5$ kV. It shows various emissions originating mainly from the following reactive species: OH($A^2\Sigma^+ - X^2\Pi$) around 309 nm, N₂(SPS) at 337.1 nm ($C^3\Pi_u - B^3\Pi_g$ transition), N₂⁺(FNS) at 391.4 nm ($B^2\Sigma_u^+ - X^2\Sigma_g^+$), various excited helium lines (i.e., He($3^1P - 2^1S$) at 501.5 nm, He($3^3D - 2^3P$) at 587.5 nm, He($3^1D - 2^1P$) at 667.8 nm, He($3^3S - 2^3P$) at 706.5 nm, and He($3^1S - 2^1P$) at 728.1 nm), atomic excited oxygen ($O^5P - 5S$) at 777 nm), and hydrogen (H_α at 656.3 nm). Additionally, very weak emissions of N₂(FPS) are detected, which are indicative of the production of N₂(A) metastables due to the radiative transition $B^3\Pi_g - A^3\Sigma_u^+$. N₂(A) are key species in DBD-based discharges, since they stimulate various chemical reactions, leading to the production of reactive species, such as NO_γ, OH(A), N₂(B), N₂(C), etc. On the other hand, the detection of N₂⁺(FNS) indicates the presence of He metastables (He_m) and helium dimer ions (He₂⁺) in the GIWs, which are believed to play a crucial role in the dynamics of guided streamers. He_m are created through collisional excitation of the ground state helium with electrons, or radiative de-excitations of higher energy levels of helium. Besides, He₂⁺ are formed via three-body reactions ($He^+ + 2He \rightarrow He_2^+ + He$ [16]). Both of the species contribute to the excitation of nitrogen ions due to the following reactions [16,43]:

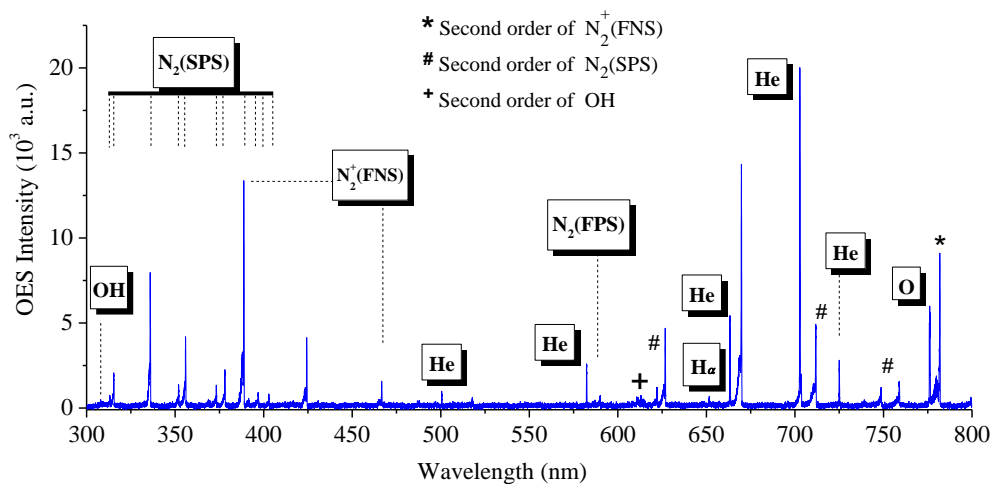
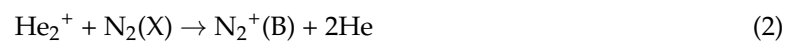


Figure 11. Typical wide optical emission spectrum of the GIWs used for the identification of the emissive reactive species generated in GIWs (the spectrum is not calibrated in terms of irradiance and any comparison between different species intensities should be avoided). The optical fiber collects the emitted light from the entire GIWs length (0.5 cm). Operating conditions: $Q = 3$ slm, $V_p = 4.5$ kV, $d = 2\%$ and $f = 15$ kHz.

Furthermore, OH(A) molecules are produced via dissociation (through collisions with electrons) of H₂O molecules (present in the form of vapors) and electron impact excitation of the OH(X) [14]. N₂(C) is produced through the electron impact excitation of N₂(X) species, later forming N₂(SPS) through radiative relaxation to the N₂(B) state. Excited atomic H and O are due to electron impact

excitation of their corresponding ground states, which are formed by the dissociation of O₂ (stands only for O) and water vapour (stands for O and H).

The possibility of tuning/enhancing the chemical reactivity of GIWs that are generated with the present device is considered herein by varying the applied voltage amplitude from 6 to 8 kV (idem with the previous sections). Its effect on the intensities of representative chemical species is shown in Figure 12. It is underlined that the spectroscopic system is not calibrated in terms of relative irradiance, which is out of the purpose of the present study. Thus, a comparison between the different species intensities should be avoided. Nevertheless, this should not affect the qualitative analysis of species intensities versus V_p . The upper frames of Figure 12 show the evolution versus the voltage amplitude of characteristic structures of representative molecular bands and atomic lines, which were considered for the analysis. In the lower frame of Figure 12, species maximum intensities are plotted versus the voltage amplitude. As it can be seen, all of the intensities rise almost linearly with the increment of the voltage amplitude from 6 to 8 kV, which was verified by fitting the related transitions with linear functions (solid lines). The rising slopes of the fitting curves are not the same, which implies different production mechanisms of these species. These variations are in quite good agreement with the ones that were obtained in Figure 5, where I_{Peak} and Q_{main} grew also linearly with the voltage amplitude and other published works concerning identical [16,25] and different [43] GIWs setups. This increase of I_{Peak} and Q_{main} was attributed to the higher electrical energy delivered in the reactor at elevated voltage amplitudes. The electrons gain more energy inducing additional avalanches as compared with the ones at lower voltage amplitudes, which eventually lead to faster excitations/ionizations and enhanced species densities, both in the inter-electrode section and the gaseous channel. In Figure 12 (lower frame), this is well confirmed, since amplified intensities of reactive emissive species are achieved with increasing V_p . The chemical reactivity can be also tuned by varying either the duty cycle or the frequency of the pulsed voltage (not shown here), and this, for temperature values that are not harmful for the reactor mechanical components and the biological samples.

The above variations imply modifications on the electron temperature (T_e) in GIWs. T_e could be approximated (under LTE conditions) via the electron excitation temperature, obtained using the well-known Boltzmann-plot method from the emission intensities of different helium lines detected in the spectrum [20,46–48]. Its determination could support further the above statements. Unfortunately, it was not possible to calculate the excitation temperature (T_{exc}) in our experiments since the spectral response of the entire optical system was not known, and any deduced value would be obviously outlier. This was due to unavailability of any adequate equipment (calibrated light source and integrating sphere), which would allow the performance of radiometrically calibrated measurements. However, based on different published works [20,46–48], an estimation of T_{exc} can be made by comparing T_{exc} values measured for similar GIWs like the present one. For instance, T_{exc} was calculated by Walsh et al. [46] for helium GIWs that were generated with a single-electrode linear-field reactor operating with RF voltage. It was found to be 0.99 eV, and it provided a rough estimation of the T_e in their case. Xiong et al. [47] characterized by means of absolutely calibrated emission spectroscopy a coaxial-geometry helium GIW in contact with a metal plate, operating with μ s-pulsed high voltage at 2 kHz. T_{exc} was found to be about 1.2 eV at 12 kV, while it increased with the voltage amplitude. Besides, the electron density (n_e), calculated via the Stark broadening of two emission lines (i.e., He at 447.1 and H β at 486.1 nm), increased with the applied voltage and varied between $\sim 10^{14}$ (center of the discharge) and $\sim 10^{15}$ cm⁻³ (edge of the discharge). In another example, Jögi et al. [20] investigated a helium linear-field “micro-plasma jet” that was generated within microtubes (diameter– D_{tube} : 80–500 μ m) and biased by sinusoidal high voltage at 6 kHz. The calculated T_{exc} was ~ 0.23 eV for $D_{tube} = 80$ μ m and it decreased down to ~ 0.17 eV with increasing D_{tube} . The same tendency versus D_{tube} was recorded for n_e (measured via Stark broadening of H β line at 486.1 nm), which was found to be $\sim 10^{14}$ cm⁻³ for $D_{tube} = 500$ μ m. These T_{exc} values were in good agreement with the ones that were measured by Joh et al. [48] for a helium/oxygen “APPJ” driven with μ s-pulsed high voltage (1.8 kV/50 kHz). Finally, Chang et al. [49] managed to measure T_e (1.87 eV) in a linear-field helium GIW that was driven with

sinusoidal voltage (8.9 kV/17 kHz). For the calculation, they used the EEDF by combining the ions number balance with the gas temperature (320 K in their case). This value is very close to the one accurately measured by Sousa et al. [50] via Thomson Scattering (up to 2 eV). The previous T_{exc} values differ between them, which could be attributed to the strong deviation of the atomic state distribution function from thermodynamic equilibrium in GIWs [20]. Also, the different geometries, operating conditions, and the presence of targets (conductive/insulating/floating potential) could play a certain role on the value of T_{exc} [50]. Since the present GIWs device presents lots of similarities with the previous ones (geometry, operation at atmospheric pressure, voltage/frequency, operating gas, etc.) it is expected that T_{exc} lies in the range of the abovementioned values. On the other hand, it is assumed that T_e is not far from the one measured by Chang et al. [49] since the gas temperature (T_{gas}) in our case is found to be 344 K (value taken for $V_p = 8$ kV, $d = 2\%$ and $f = 10$ kHz, see Figure 13 for details) and the setups are similar.

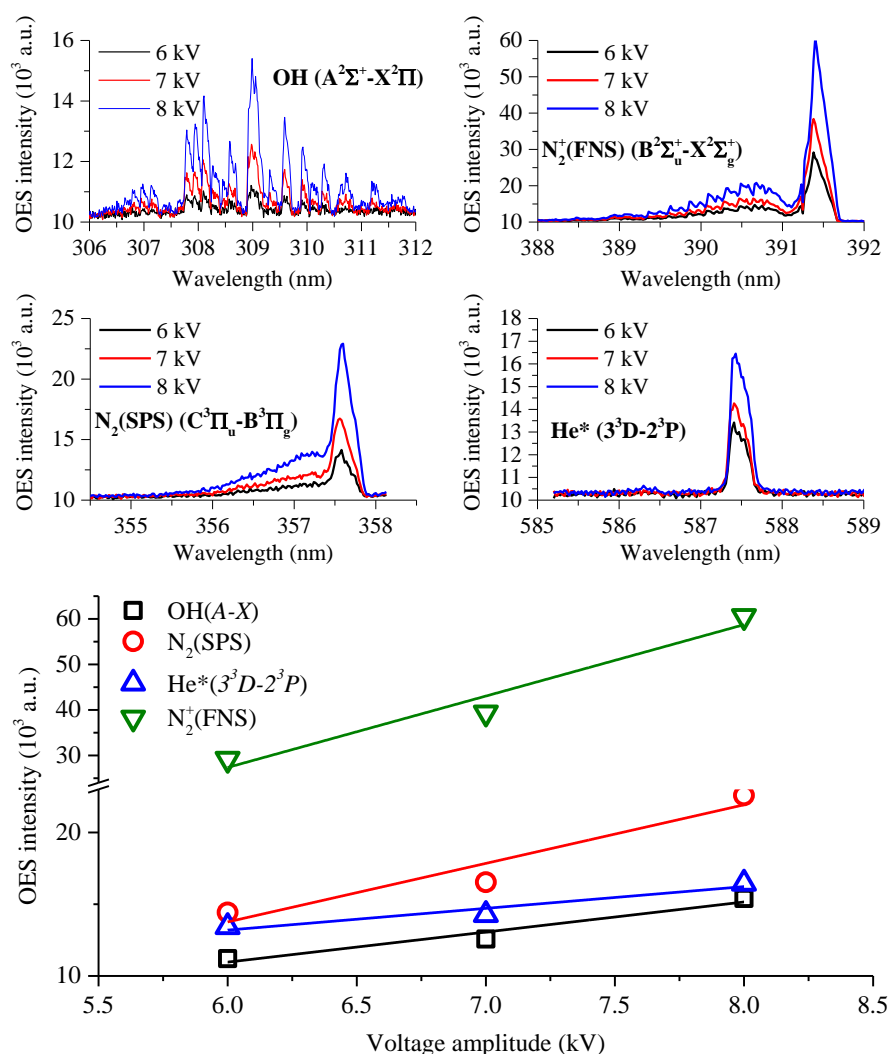


Figure 12. Upper frame: representative molecular bands and atomic lines of principal reactive emissive species (OH(A-X)—309 nm, N₂(SPS)—337.1 nm, N₂⁺(FNS)—391.4 nm and excited He—587.5 nm) detected in the GIWs spectrum versus the voltage amplitude. Species intensities are integrated in space (0.5 cm—zone starting from the tube nozzle) and time (within 1500 voltage pulses). **Lower frame:** maximum emission intensities of the aforementioned species (scatter symbols) as functions of the voltage amplitude, fitted with linear functions (solids lines). Operating conditions: $Q = 3$ slm, $d = 2\%$ and $f = 15$ kHz.

The important modifications of the dielectric tube temperature, which were demonstrated in the previous sections (see Figures 7 and 10), are characteristic of the changes on the gas temperature (T_{gas}) during the operation of GIWs. In typical GIWs experiments, T_{gas} is usually estimated from the rotational temperature (T_{rot}) of probe molecules, such as the OH(A) around 309 nm [6,15,46,47,49]. In our case, OH(A-X) emission was detected in the emission spectrum of GIWs (see Figure 11). A representative experimental rotational structure of this molecule is given in Figure 13 (black color), which was fitted with the corresponding synthetic rotational spectrum (red dots) that was produced with a home-made code [6,14,15,51]. T_{rot} was obtained as the value giving the best fit between these two spectra based on the least squares method. The fitting gives $T_{\text{rot}} = T_{\text{gas}} = 344$ K. The error on the measured value is estimated to be ± 40 K [14]. Any influence on the measured value due to the spectral response of the optical system is excluded, since the latter is expected to be nearly constant within such a small wavelength interval (6 nm). In Figure 13, T_{rot} was measured for $V_p = 8$ kV, $f = 10$ kHz, and $d = 2\%$. When compared with T_{sat} in Figure 10 (at the same conditions), it is ~ 15 K higher. This could be possible due to heat dissipation in the tube walls during plasma operation. Besides that, the evolutions of the gas temperature were similar to the ones of T_{sat} , validating the results of Figures 7 and 10. Thus, special care should be taken for selecting adequate operating conditions of GIWs for biomedical applications and reactor proper functionality. Using the measured T_{gas} from Figure 13 and the electron density of the plasma, the ionization degree can be estimated under our experimental conditions, as it is shown below.

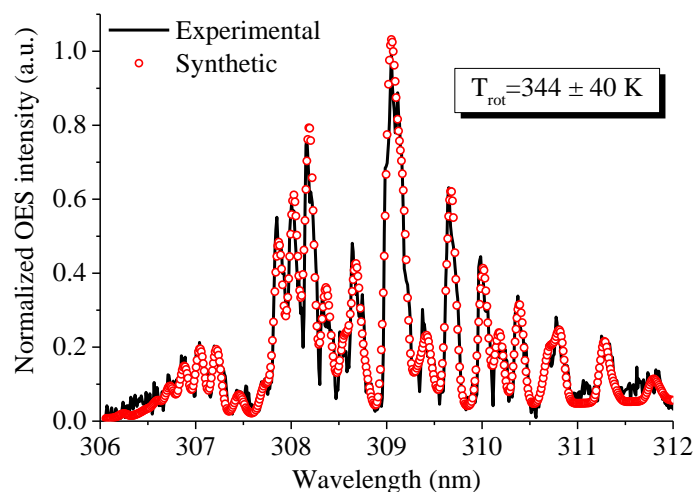


Figure 13. Synthetic (red dots) rotational distribution of the OH(A) molecule around 309 nm fitted to the corresponding experimental one (black) for the determination of the gas temperature. ($Q = 3$ slm, $V_p = 8$ kV, $f = 10$ kHz and $d = 2\%$).

Concerning the electron density of GIWs that were generated with the present device, an approximation was made by our group using a modified version of the related DBD reactor (i.e., single-electrode linear-field geometry) [32]. The device was operated in pure helium at 2 slm and driven with sinusoidal high voltage (20 kV p-p, 10 kHz). Measuring the amplitude of sharp current impulses (1 mA) superimposed on the capacitive current and using the propagation velocity of the GIWs (2.5×10^4 m s $^{-1}$) as the electron drift velocity in the well-known formula of the current density, n_e was found to be $\sim 2.5 \times 10^{11}$ cm $^{-3}$. Of course, this is a rough estimation of n_e and it represents a lower limit as compared with the higher values measured using more accurate methods, like Thomson Scattering [50]. Indeed, using TS technique in a helium pulsed GIW (like the present one), Sousa et al. [50] measured electron density values of up to 2×10^{13} cm $^{-3}$, which are lower than the ones listed in the previous paragraph and higher than the one estimated in our case. Adopting the

(maximum) more-accurate value of Sousa et al. [50], the ionization degree of the present GIW could be estimated via the Formula (3):

$$\alpha = \frac{n_e}{n_e + n_N} \quad (3)$$

where $n_N = P/k_b \times T_{\text{gas}} \approx 2.133 \times 10^{19} \text{ cm}^{-3}$ is the number density of neutrals at atmospheric pressure and $T_{\text{gas}} = 344 \text{ K}$ in our case (see Figure 13). By simple numerical application in (1), α is found to be $\sim 4.7 \times 10^{-7}$, which is typical for GIWs. The ions density is expected to be similar with the one of electrons. In any case, it is underlined that the accurate determination of the electron temperature/density, is out of the purpose of the present work, which aims to define adequate operational regimes for various applications controlling (especially) the poorly investigated thermal processes that are involved in GIWs.

4. Conclusions

In the present work, the thermal, electrical, and optical characteristics of GIWs produced with a linear-field compact DBD-based reactor, were thoroughly investigated. The main advantages of the present device are that it operates effectively in helium with μs -pulsed and sinusoidal high voltage, it is of very simple geometry and it can be fabricated effortlessly. Herein, the reliable operation of the reactor was demonstrated under μs -pulsed positive high voltage conditions. Many GIWs systems presented in the literature, similar (more-or-less) with the present one, are considered as a-priori cold under commonly adopted operating conditions (i.e., GIWs formed in noble gases with DBD reactors driven by audio-frequency high voltage of few kV in amplitude). This issue has motivated the present work, which consists of a systematic investigation of the thermal processes evolved during GIWs operation. Except the effect of the main parameters of the power supply (voltage amplitude, duty cycle, and frequency) on the maximum steady-state temperature of the dielectric tube (T_{sat}) and the gas temperature, their influence on different current-related quantities (I_{Peak} , Q_{main} , and Δt_{GIWs}), and on the GIWs visible propagation length, was investigated. In addition, optical emission spectroscopy was employed to identify the reactive species that were generated outside the reactor. The obtained results revealed that the device could be easily parameterized in terms of temperature, current amplitude, GIWs propagation length, and controllable production of reactive emissive species. Based on these results, appropriate operational windows were defined to avoid reactor malfunctioning due to high operational temperatures and to produce on-demand GIWs for fundamental studies, biomedical applications and inert material treatments.

More specifically, the produced GIWs reached maximum lengths of up to 4 cm for low duty cycle values (1–2%) and high amplitudes of the applied voltage (8 kV) and frequency (15–20 kHz). Besides, T_{sat} varied between 25 and 80 °C, while it increased linearly with the voltage amplitude. The effects of the duty cycle and the frequency were less significant, especially at low voltage amplitudes. Accordingly, not all of the operational regimes are adequate for thermal-free operation, which is crucial for biomedical applications, implying that special care should be taken when applying GIWs on heat-sensitive specimens. In this work, the real-time measurement of the tube temperature and the determination of steady-state values allowed for the effective control of the thermal processes that are involved in the DBD reactor during plasma operation. Furthermore, due to the propagation of fast guided streamers outside the reactor (i.e., abundance of N_2 and O_2), highly reactive species were generated in the emission spectrum of GIWs, which were detected and identified (OH, $\text{N}_2(\text{SPS})$, $\text{N}_2^+(\text{FNS})$, excited He/O/H, and $\text{N}_2(\text{FPS})$). The possibility of controlling/enhancing the species production was demonstrated by analyzing the effect of the voltage amplitude on representative transitions. Among these species, particularly OH and O radicals are of great importance for biomedical applications, since they are highly oxidative. Furthermore, the presence of He metastables and He_2^+ ions was suggested, which are responsible for the production of the $\text{N}_2^+(\text{B})$, thus stimulating the discharge dynamics. Within the range of parameters considered herein, it is possible to define various

operational windows (i.e., short/long “plasma plumes” of enhanced/moderate chemical reactivity at low temperatures) for targeted plasma-based applications.

Acknowledgments: The present work has been supported by the Mediterranean Office of Youth (mobility scholarship obtained by Kristaq Gazeli for PhD studies in France, labeled program No. 2010/040/02) and the French Agence National de la Recherche (ANR, post-doc funding obtained by Le Thanh Doanh in the frame of the ANR program PLASMAVIV).

Author Contributions: Franck Clément and Bernard Held conceived and designed the experiments; Le Thanh Doanh performed the electrical and spectroscopic measurements and Kristaq Gazeli performed the temperature and imaging experiments; Le Thanh Doanh analyzed the data; Kristaq Gazeli and Franck Clément wrote the paper.

Conflicts of Interest: The authors declare no conflict of interest. The founding sponsors had no role in the design of the study; in the collection, analyses, or interpretation of data; in the writing of the manuscript, and in the decision to publish the results.

References

1. Iza, F.; Kim, G.J.; Lee, S.M.; Lee, J.K.; Walsh, J.L.; Zhang, Y.T.; Kong, M.G. Microplasmas: Sources, particle kinetics, and biomedical applications. *Plasma Process. Polym.* **2008**, *5*, 322–344. [[CrossRef](#)]
2. Lu, X.; Laroussi, M.; Puech, V. On atmospheric-pressure non-equilibrium plasma jets and plasma bullets. *Plasma Sources Sci. Technol.* **2012**, *21*, 034005. [[CrossRef](#)]
3. Boeuf, J.-P.; Yang, L.L.; Pitchford, L.C. Dynamics of a guided streamer (“plasma bullet”) in a helium jet in air at atmospheric pressure. *J. Phys. D* **2013**, *46*, 015201. [[CrossRef](#)]
4. Lu, X.; Naidis, G.V.; Laroussi, M.; Ostrikov, K. Guided ionization waves: Theory and experiments. *Phys. Rep.* **2014**, *540*, 123–166. [[CrossRef](#)]
5. Robert, E.; Sarron, V.; Riès, D.; Dozias, S.; Vandamme, M.; Pouvesle, J.-M. Characterization of pulsed atmospheric-pressure plasma streams (PAPS) generated by a plasma gun. *Plasma Sources Sci. Technol.* **2012**, *21*, 034017. [[CrossRef](#)]
6. Gazeli, K.; Svarnas, P.; Vafeas, P.; Papadopoulos, P.K.; Gkelios, A.; Clément, F. Investigation on streamers propagating into a helium jet in air at atmospheric pressure: Electrical and optical emission analysis. *J. Appl. Phys.* **2013**, *114*, 103304. [[CrossRef](#)]
7. Talviste, R.; Jõgi, I.; Raud, J.; Paris, P. The effect of dielectric tube diameter on the propagation velocity of ionization waves in a He atmospheric-pressure micro-plasma jet. *J. Phys. D* **2016**, *49*, 195201. [[CrossRef](#)]
8. Xiong, Z.; Robert, E.; Sarron, V.; Pouvesle, J.-M.; Kushner, M.J. Atmospheric-pressure plasma transfer across dielectric channels and tubes. *J. Phys. D* **2012**, *45*, 275201. [[CrossRef](#)]
9. Naidis, G.V. Modelling of streamer propagation in atmospheric-pressure helium plasma jets. *J. Phys. D* **2010**, *43*, 402001. [[CrossRef](#)]
10. Von Woedtke, T.; Reuter, S.; Masur, K.; Weltmann, K. Plasmas for medicine. *Phys. Rep.* **2013**, *530*, 291–320. [[CrossRef](#)]
11. Tanaka, H.; Ishikawa, K.; Mizuno, M.; Toyokuni, S.; Kajiyama, H.; Kikkawa, F.; Metelmann, H.-R.; Hori, M. State of the art in medical applications using non-thermal atmospheric pressure plasma. *Rev. Mod. Plasma Phys.* **2017**, *1*. [[CrossRef](#)]
12. Kim, S.J.; Chung, T.H. Cold atmospheric plasma jet-generated RONS and their selective effects on normal and carcinoma cells. *Sci. Rep.* **2016**, *6*, 20332. [[CrossRef](#)] [[PubMed](#)]
13. Svarnas, P.; Matrali, S.H.; Gazeli, K.; Aleiferis, S.; Clément, F.; Antimisiaris, S.G. Atmospheric-pressure guided streamers for liposomal membrane disruption. *Appl. Phys. Lett.* **2012**, *101*, 264103. [[CrossRef](#)]
14. Gazeli, K.; Noël, C.; Clément, F.; Daugé, C.; Svarnas, P.; Belmonte, T. A study of atmospheric-pressure guided streamers for potential biological applications. *Plasma Sources Sci. Technol.* **2013**, *22*, 025020. [[CrossRef](#)]
15. Gazeli, K.; Svarnas, P.; Held, B.; Marlin, L.; Clément, F. Possibility of controlling the chemical pattern of He and Ar “guided streamers” by means of N₂ or O₂ additives. *J. Appl. Phys.* **2015**, *117*, 093302. [[CrossRef](#)]
16. Jarrige, J.; Laroussi, M.; Karakas, E. Formation and dynamics of plasma bullets in a non-thermal plasma jet: Influence of the high-voltage parameters on the plume characteristics. *Plasma Sources Sci. Technol.* **2010**, *19*, 065005. [[CrossRef](#)]

17. Zhu, P.; Meng, Z.; Hu, H.; Ouyang, J. Effect of external electric and magnetic field on propagation of atmospheric pressure plasma jet. *Phys. Plasmas* **2017**, *24*, 103512. [[CrossRef](#)]
18. Vasile Nastuta, A.; Pohoata, V.; Topala, I. Atmospheric pressure plasma jet-Living tissue interface: Electrical, optical, and spectral characterization. *J. Appl. Phys.* **2013**, *113*, 183302. [[CrossRef](#)]
19. Walsh, J.L.; Kong, M.G. Room-temperature atmospheric pressure argon plasma jet sustained with submicrosecond high-voltage pulses. *Appl. Phys. Lett.* **2007**, *91*, 221502. [[CrossRef](#)]
20. Jōgi, I.; Talviste, R.; Raud, J.; Piip, K.; Paris, P. The influence of tube diameter on the properties of an atmospheric pressure He micro-plasma jet. *J. Phys. D* **2014**, *47*, 415202. [[CrossRef](#)]
21. Robert, E.; Barbosa, E.; Dozias, S.; Vandamme, M.; Cachoncinlle, C.; Viladrosa, R.; Pouvesle, J.-M. Experimental study of a compact nanosecond plasma gun. *Plasma Process. Polym.* **2009**, *6*, 795–802. [[CrossRef](#)]
22. Xiong, Z.; Kushner, M. Atmospheric pressure ionization waves propagating through a flexible high aspect ratio capillary channel and impinging upon a target. *Plasma Sources Sci. Technol.* **2012**, *21*, 034001. [[CrossRef](#)]
23. Karakas, E.; Akman, M.A.; Laroussi, M. The evolution of atmospheric-pressure low-temperature plasma jets: Jet current measurements. *Plasma Sources Sci. Technol.* **2012**, *21*, 034016. [[CrossRef](#)]
24. Gerber, I.C.; Mihaila, I.; Hein, D.; Nastuta, A.V.; Jijie, R.; Pohoata, V.; Topala, I. Time behavior of helium atmospheric pressure plasma jet electrical and optical parameters. *Appl. Sci.* **2017**, *7*, 812. [[CrossRef](#)]
25. Uchida, G.; Takenaka, K.; Setsuhara, Y. Effects of discharge voltage waveform on the discharge characteristics in a helium atmospheric plasma jet. *J. Appl. Phys.* **2015**, *117*, 153301. [[CrossRef](#)]
26. Yonemori, S.; Ono, R. Effect of discharge polarity on the propagation of atmospheric-pressure helium plasma jets and the densities of OH, NO, and O radicals. *Biointerphases* **2015**, *10*, 029514. [[CrossRef](#)] [[PubMed](#)]
27. Lu, X.; Laroussi, M. Dynamics of an atmospheric pressure plasma plume generated by submicrosecond voltage pulses. *J. Appl. Phys.* **2006**, *100*, 063302. [[CrossRef](#)]
28. Jiang, N.; Ji, A.; Cao, Z. Atmospheric pressure plasma jet: Effect of electrode configuration, discharge behavior, and its formation mechanism. *J. Appl. Phys.* **2009**, *106*, 013308. [[CrossRef](#)]
29. Mericam-Bourdet, N.; Laroussi, M.; Begum, A.; Karakas, E. Experimental investigations of plasma bullets. *J. Phys. D* **2009**, *42*, 055207. [[CrossRef](#)]
30. Karakas, E.; Laroussi, M. Experimental studies on the plasma bullet propagation and its inhibition. *J. Appl. Phys.* **2010**, *108*, 063305. [[CrossRef](#)]
31. Karakas, E.; Koklu, M.; Laroussi, M. Correlation between helium mole fraction and plasma bullet propagation in low temperature plasma jets. *J. Phys. D* **2010**, *43*, 155202. [[CrossRef](#)]
32. Papadopoulos, P.K.; Vafeas, P.; Svarnas, P.; Gazeli, K.; Hatzikonstantinou, P.M.; Gkelios, A.; Clément, F. Interpretation of the gas flow field modification induced by guided streamer (“plasma bullet”) propagation. *J. Phys. D* **2014**, *47*, 425203. [[CrossRef](#)]
33. Nastuta, A.V.; Topala, I.; Grigoras, C.; Pohoata, V.; Popa, G. Stimulation of wound healing by helium atmospheric pressure plasma treatment. *J. Phys. D* **2011**, *44*, 105204. [[CrossRef](#)]
34. Walsh, J.L.; Iza, F.; Janson, N.B.; Law, V.J.; Kong, M.G. Three distinct modes in a cold atmospheric pressure plasma jet. *J. Phys. D Appl. Phys.* **2010**, *43*, 075201. [[CrossRef](#)]
35. Zhu, W.-C.; Li, Q.; Zhu, X.-M.; Pu, Y.-K. Characteristics of atmospheric pressure plasma jets emerging into ambient air and helium. *J. Phys. D Appl. Phys.* **2009**, *42*, 202002. [[CrossRef](#)]
36. Li, Q.; Li, J.; Zhu, W.-C.; Zhu, X.; Pu, Y. Effects of gas flow rate on the length of atmospheric pressure nonequilibrium plasma jets. *Appl. Phys. Lett.* **2009**, *95*, 141502. [[CrossRef](#)]
37. Darny, T.; Pouvesle, J.-M.; Puech, V.; Douat, C.; Dozias, S.; Robert, E. Analysis of conductive target influence in plasma jet experiments through helium metastable and electric field measurements. *Plasma Sources Sci. Technol.* **2017**, *26*, 045008. [[CrossRef](#)]
38. Yamada, H.; Sakakita, H.; Kato, S.; Kim, J.; Kiyama, S.; Fujiwara, M.; Itagaki, H.; Okazaki, T.; Ikehara, S.; Nakanishi, H.; et al. Spectroscopy of reactive species produced by low-energy atmospheric-pressure plasma on conductive target material surface. *J. Phys. D* **2016**, *49*, 394001. [[CrossRef](#)]
39. Es-Sebbar, E.-T.; Gazeli, K.; Bauville, G.; Fleury, M.; Neveu, O.; Pasquiers, S.; Santos Sousa, J. Argon metastable density in an atmospheric microplasma jet in interaction with a dielectric surface. In Proceedings of the 19th International Conference on Atomic Processes in Plasmas (APiP), Paris, France, 4–8 April 2016.
40. Gazeli, K.; Bauville, G.; Fleury, M.; Neveu, O.; Jeanney, P.; Pasquiers, S.; Santos Sousa, J. Radial and temporal density profiles of Ar(1s5) metastables in a nanosecond pulsed plasma jet impinging on different dielectric surfaces. In Proceedings of the XXXIII ICPIG Conference, Lisbon, Portugal, 9–14 July 2017.

41. Hsu, Y.; Yang, Y.; Wu, C.; Hsu, C. Downstream characterization of an atmospheric pressure pulsed arc jet. *Plasma Chem. Plasma Process.* **2010**, *30*, 363–372. [[CrossRef](#)]
42. Xiong, Q.; Lu, X.; Ostrikov, K.; Xiong, Z.; Xian, Y.; Zhou, F.; Zou, C.; Hu, J.; Gong, W.; Jiang, Z. Length control of He plasma jet plumes: Effects of discharge parameters and ambient air. *Phys. Plasmas* **2009**, *16*, 043505. [[CrossRef](#)]
43. Xiong, Q.; Lu, X.; Xian, Y.; Liu, J.; Zou, C.; Xiong, Z.; Gong, W.; Chen, K.; Pei, X.; Zou, F.; et al. Experimental investigations on the propagation of the plasma jet in the open air. *J. Appl. Phys.* **2010**, *107*, 073302. [[CrossRef](#)]
44. Walsh, J.L.; Olszewski, P.; Bradley, J.W. The manipulation of atmospheric pressure dielectric barrier plasma jets. *Plasma Sources Sci. Technol.* **2012**, *21*, 34007. [[CrossRef](#)]
45. Wu, S.; Xu, H.; Lu, X.; Pan, Y. Effect of pulse rising time of pulse dc voltage on atmospheric pressure non-equilibrium plasma. *Plasma Process. Polym.* **2013**, *10*, 136–140. [[CrossRef](#)]
46. Walsh, J.L.; Kong, M.G. Contrasting characteristics of linear-filed and cross-field atmospheric plasma jets. *Appl. Phys. Lett.* **2008**, *93*, 111501. [[CrossRef](#)]
47. Xiong, Q.; Nikiforov, A.; Gonzalez, M.A.; Leys, C.; Lu, X.P. Characterization of an atmospheric helium plasma jet by relative and absolute optical emission spectroscopy. *Plasma Sources Sci. Technol.* **2013**, *22*, 015011. [[CrossRef](#)]
48. Joh, H.M.; Choi, J.Y.; Kim, S.J.; Chung, T.H.; Kang, T.-H. Effect of additive oxygen gas on cellular response of lung cancer cells induced by atmospheric pressure helium plasma jet. *Sci. Rep.* **2014**, *4*, 6638. [[CrossRef](#)] [[PubMed](#)]
49. Chang, Z.-S.; Zhang, C.-J.; Shao, X.-J.; Zhang, Z.-H. Diagnosis of gas temperature, electron temperature, and electron density in helium atmospheric pressure plasma jet. *Phys. Plasmas* **2012**, *19*, 073513. [[CrossRef](#)]
50. Santos Sousa, J.; Hübner, S.; Sobota, A.; Pasquiers, S.; Puech, V.; Sadeghi, N. Electron properties in atmospheric pressure plasma jets determined by Thomson scattering. In Proceedings of the XXIII ESCAMPIG Conference, Bratislava, Slovakia, 12–16 July 2016.
51. Cardoso, R.P.; Belmonte, T.; Keravec, P.; Kosior, F.; Henrion, G. Influence of impurities on the temperature of an atmospheric helium plasma in microwave resonant cavity. *J. Phys. D* **2007**, *40*, 1394–1400. [[CrossRef](#)]



© 2017 by the authors. Licensee MDPI, Basel, Switzerland. This article is an open access article distributed under the terms and conditions of the Creative Commons Attribution (CC BY) license (<http://creativecommons.org/licenses/by/4.0/>).